Fuel 89 (2010) 1928–1935

Contents lists available at ScienceDirect

Fuel

journal homepage: www.elsevier.com/locate/fuel

Quasi-1D and 3D TPOX porous media diffuser reformer model

J.M.C. Pereira [a], M.A.A. Mendes [a], D. Trimis [b], J.C.F. Pereira [a,*]

[a] *Technical University of Lisbon, Instituto Superior Técnico, Mech. Eng. Dept., LASEF, Av. Rovisco Pais 1, 1049-001 Lisbon, Portugal*
[b] *Technische Universität Bergakademie Freiberg, Institute of Thermal Engineering, Gustav-Zeuner-Str. 7, 09596 Freiberg, Germany*

ARTICLE INFO

Article history:
Received 26 May 2009
Received in revised form 16 December 2009
Accepted 7 January 2010
Available online 19 January 2010

Keywords:
Reforming
Porous media
Combustion modeling
Hydrogen production
Fluid flow

ABSTRACT

This paper focuses on the numerical simulations of methane thermal partial oxidation reforming process within inert porous media and their comparison with experiments. In order to produce hydrogen rich mixtures and for the sake of reaction stability, the reformer consists on a diffuser filled with porous media. The validity of using a *quasi*-1D approach to model this system is explored based on 3D simulations of the isothermal fluid flow through the porous solid structure. Several fluid flow cases were taken into account as well as two different porous materials, Al_2O_3 fiber lamellae and SiSiC foam. The detailed fluid flow information obtained from the 3D study was used to provide the realistic cross-sectional area variation of the *quasi*-1D model. The *quasi*-1D 12-steps reduced chemistry model predictions are in very satisfactory agreement with the temperature and concentration fields measured within the diffuser porous reformer.

1. Introduction

Nowadays there is an increasing interest on developing systems relying on renewable energy sources to diminish the dependence on fossil fuel reserves and to increase environmental quality. Hydrogen is thought as a potential energy carrier for a sustainable energy supply owing to its flexible production from many different primary energy sources and non-polluting characteristics. Unfortunately, hydrogen is not readily accessible in its pure form and hence has to be produced from atomic bounded hydrogen in available sources, e.g., water, hydrocarbons, etc. In order to gradually convert the actual energy generation systems from conventional to renewable a smooth transition is required, consequently, today pure hydrogen must be produced from hydrocarbons (mainly fossil fuels) to meet the actual energy demand [1].

Among the existing processes to produce hydrogen from hydrocarbon fuels, the reforming of hydrocarbons to synthesis-gas (consisting mainly of hydrogen and carbon monoxide) is the most common one. Compared with other reforming technologies, the thermal partial oxidation (TPOX) process offers several advantages [2,3], such as, no need for external heat sources and additional feeds like water as in steam reforming; absence of catalysts which eliminates the catalyst deactivation problems; good dynamic response; and applicability to almost all hydrocarbons. However, the main drawbacks are the comparatively low hydrogen yield and the tendency to produce soot.

Due to the slow chemical kinetics and decreased flame stability at low adiabatic flame temperatures existing in the TPOX process, the use of inert porous media (IPM) to built reformers is seen as a promising practical solution [4,5]. The combustion within IPM benefits from the higher heat recirculation provided by the solid matrix, which results in higher local combustion temperatures [6]. This increases the burning velocity and the flame stability of the TPOX process improving its operational characteristics [4].

There are various techniques to stabilize a combustion process within IPM available [7]. One possibility is to make use of thermal flame quenching, where the flame is stabilized between two distinct porous media zones [8]. The porous material in the upstream region presents small pores preventing combustion to occur due to the sub-critical Péclet number. Therefore, combustion can only exist in the downstream region where the porous material is made of larger pores and shows a supercritical Péclet number. Another possibility to stabilize the combustion within IPM is to induce a change of the flow speed by a continuous variation of the cross-sectional area [7]. This creates an upstream region with a small cross-sectional area, where the flow velocity is much higher than the burning velocity preventing flashback to occur, and owing to the increase of the cross-sectional area in the downstream direction, there exist a kinematic equilibrium position where the flow velocity equals the burning velocity and the flame can be stabilized. The two flame stabilization techniques explained above were successfully applied to the TPOX process within IPM. The cross-sectional area variation technique was used in [4] and the thermal flame quenching technique was applied in [5]. Both techniques are shown to work, however the cross-sectional area variation technique was preferred in [4] due to the extremely high reactant

* Corresponding author. Tel.: +351 218417928.
E-mail address: jcfpereira@ist.utl.pt (J.C.F. Pereira).

0016-2361/$ - see front matter © 2010 Elsevier Ltd. All rights reserved.
doi:10.1016/j.fuel.2010.01.011

Nomenclature

Latin

t	time coordinate
x	axial distance coordinate
A	cross-section area
u	bulk gas velocity
v	species diffusion velocity
Y	species mass fraction
T	temperature
MW	species molar weight
C_p	specific heat capacity at constant pressure
h	species enthalpy
H_v	volumetric heat transfer coefficient
Q_r	radiative heat flux
a_v	specific surface area
d_p	porous structure characteristic dimension
C, n	constants of convective heat transfer correlation
Nu	Nusselt number
Re	Reynolds number

Greek

ϕ	porosity
ρ	density
$\dot{\omega}$	species production rate
λ	thermal conductivity; air/fuel ratio
β	extinction coefficient
ω	scattering albedo
ε	emissivity
μ	dynamic viscosity
σ	Stefan–Boltzmann constant

Subscripts

g	gas mixture
s	solid
k	species k in gas mixture

temperatures used (in order to reduce soot formation). An effective application of the thermal flame quenching technique to the TPOX process is not allowed, because there exists a potential danger of self-ignition of the reactants in the upstream porous media region.

Numerical simulations of combustion within IPM burners have been widely performed with different modeling complexity levels depending on the desired information and on computational limitations. Generally, multi-dimensional (MD) simulations have been performed using reduced reaction mechanisms [9–11] to predict temperature distributions and some species in complex burner geometries. Detailed reaction mechanisms have also been used [12–14], allowing a more accurate prediction of some particular species, e.g. pollutants, but the increased complexity of these models can create some convergence and time consuming problems. Simulations using one-dimensional (1D) models were generally performed for simple burner geometries [15,16], and here the detailed reaction mechanisms are less problematic and are commonly used when required. In the particular case of TPOX simulations, a detailed react ion mechanism may be required to accurately predict the synthesis-gas composition. Both MD and 1D TPOX simulations have been performed using detailed reaction mechanisms, see, e.g. [12,16], respectively. In [10–14], the MD description of the fluid flow, heat and mass transport in the porous media was made by means of macroscopic volume averaged forms of the conservation equations, which is a customary procedure in the study of processes taking place within porous media [17]. The same procedure is used for 1D models [15,16].

To simulate the IPM combustion using detailed chemistry, the application of 1D models reduces the convergence and computing time problems, when compared with MD models. However, the applicability of these 1D models depends on the complexity of the burner's geometry.

The objective of this study is to simulate the methane TPOX process within an IPM reformer by using a *quasi*-1D combustion model with a 12-steps reduced chemistry. The reformer studied here was developed and tested by the Institute of Thermal Engineering of the Technical University of Freiberg [4,12,18] and its geometry consists of a conical section where the reaction front is stabilized, followed by a cylindrical section where the slower reforming reactions take place. Two different IPM were tested: Al_2O_3 fiber lamellae and SiSiC porous foam. The *quasi*-1D model was supported by a preliminary 3D study of the isothermal fluid flow though the full porous solid structure. This 3D study was performed to obtain a detailed description of the isothermal flow within the IPM, which was further used to provide the realistic cross-sectional area variation of the *quasi*-1D model. The temperature and main species predictions of the *quasi*-1D reformer model were compared with experimental results for several working conditions. This study also explores the utility of the 3D/1D coupling concept, which uses the deep understanding of the macroscopic fluid flow behavior to improve the *quasi*-1D fluid flow prediction, therefore, simplifying the modeling of IPM combustion and reducing the computation time without great loss of accuracy.

After this Introduction the paper is organized in the next sections by presenting the Reference Experiments and the Governing Equations. The presentation of the predictions, experimental data and particular analysis is done in the section concerned with the Results. The paper ends with summary Conclusions.

2. Reference experiments

The methane TPOX setup and experimental results used for comparison with the numerical predictions have been reported in detail in [18,4] so that only a summary is given here.

Experimental reformate gas samples were taken at 30, 80, 180, 240, 310, 410 and 460 mm. These samples were sent to the gas analyzers with which the major species, H_2, CO, CO_2, CH_4, O_2 and C_2H_2 (intermediate species considered as soot percursor) were measured. The concentration of H_2O was calculated from the mass balance. More details about the experimental setup and the measurement techniques can be found in [4]. The methane TPOX reactor consists on a conical diffuser geometrical configuration followed by a cylindrical region as sketched in Fig. 1. The reactor is filled with either Al_2O_3 fiber lamellae or SiSiC porous foam. For illustrative purposes, Fig. 2 shows a portion of the referred media.

Table 1 lists the experimentally investigated operating conditions that were used for comparison with the numerical predictions.

3. Governing equations

The reactive flow in the IPM reformer was simulated with a *quasi*-1D model (to take into account the cross-sectional area variation in the diffuser), which is a modified version of the PREMIX code [19]. The ceramic foam was modeled as a single continuum,

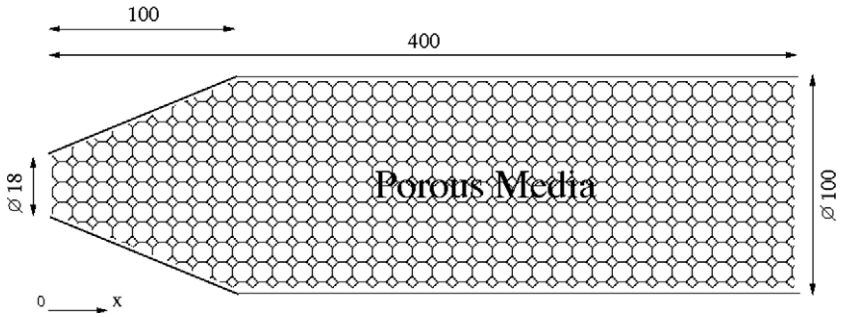

Fig. 1. Experimental TPOX reactor geometrical configuration.

Fig. 2. Al_2O_3 fiber lamellae (a) and SiSiC porous foam (b).

Table 1
Experimental conditions investigated through numerical simulations (air inlet temperature of 973 K and methane inlet temperature of 300 K with $\lambda = 0.45$).

Porous media	Case	Power (kW)
Al_2O_3	1	15
	2	20
SiSiC	3	15
	4	22

taking the averaged forms of the conservation equations. The mass and gas phase species transport are governed by Eqs. (1) and (2), respectively.

Continuity equation:

$$\frac{\partial(A\phi\rho_g)}{\partial t}+\frac{\partial(A\phi\rho_g u)}{\partial x}=0 \tag{1}$$

Species transport equation:

$$A\phi\rho_g\frac{\partial Y_k}{\partial t}+A\phi\rho_g u\frac{\partial Y_k}{\partial x}+\frac{\partial(A\phi\rho_g v_k Y_k)}{\partial x}-A\phi\dot{\omega}_k MW_k=0 \tag{2}$$

It is assumed that the reformer is adiabatic, therefore the energy equations for the gas and solid phases are given by Eqs. (3) and (4), respectively.

Gas energy equation:

$$A\phi\rho_g C_{pg}\frac{\partial T_g}{\partial t}+A\phi\rho_g uC_{pg}\frac{\partial T_g}{\partial x}-\frac{\partial}{\partial x}\left(A\phi\lambda_g\frac{\partial T_g}{\partial x}\right)+A\phi\sum_k\rho_g C_{pk}v_k\frac{\partial T_g}{\partial x}+A\phi\sum_k\dot{\omega}_k h_k MW_k+AH_v(T_g-T_s)=0 \tag{3}$$

Solid energy equation:

$$\frac{\partial(A(1-\phi)\rho_s C_{ps}T_s)}{\partial t}-\frac{\partial}{\partial x}\left(A(1-\phi)\lambda_s\frac{\partial T_s}{\partial x}\right)-AH_v(T_g-T_s)+\frac{\partial AQ_r}{\partial x}=0 \tag{4}$$

In the above equations the variables denote local intrinsic fluid phase volume averages. The porosity ϕ represents the volume fraction of the gas phase, therefore in regions outside the porous media ϕ equals 1 and Eq. (4) falls out, otherwise ϕ equals the solid porosity ϕ_s.

Both gas and solid energy equations, (3) and (4), are coupled by the convective heat transfer term $A\ H_v\ (T_g - T_s)$. The convective heat transfer coefficient H_v was obtained from the following correlation:

$$Nu=CRe^n,\quad Nu=\frac{H_v d_p}{\lambda_g a_v},\quad Re=\frac{\phi\rho_g u d_p}{\mu_g} \tag{5}$$

where C and n are constants dependent on the porous structure (see Table 2).

Table 2
Properties of both IPM used for the simulations.

IPM property	Al_2O_3 fiber lamellae	SiSiC porous foam
Porosity, ϕ	0.90	0.90
Extinction coef., β (m^{-1})	70	100
Scattering albedo, ω	0.90	0.70
Emissivity, ε	0.40	0.85
Porous structure dimension, d_p (m)	1×10^{-2}	6×10^{-4}
Specific surface area, a_v (m^2/m^3)	200	500
C in Eq. (5)	0.168	0.137
n in Eq. (5)	0.9	1.2

The boundary conditions (b.c.) used to close Eqs. (1)–(3) were Dirichlet at the inlet and Neumann at the outlet of the computational domain. For Eq. (4), the b.c. at the inlet and outlet IPM surfaces represent energy balances and are given by Eqs. (6) and (7), respectively:

$$\frac{\partial(\rho_s C_{ps} T_s)}{\partial t} dx - \lambda_s \frac{\partial T_s}{\partial x} - \frac{H_v}{a_v}(T_g - T_s) + \varepsilon\sigma(T_s^4 - T_{in}^4) = 0 \quad (6)$$

$$\frac{\partial(\rho_s C_{ps} T_s)}{\partial t} dx + \lambda_s \frac{\partial T_s}{\partial x} - \frac{H_v}{a_v}(T_g - T_s) + \varepsilon\sigma(T_s^4 - T_{out}^4) = 0 \quad (7)$$

where T_{in} and T_{out} are assumed to be equal to the inlet and outlet gas temperature, respectively.

For radiation purposes the IPM was considered as a diffuse, gray body together with a non-radiating gas mixture. The radiative heat transport term $\partial(AQ_r)/\partial x$ appearing in Eq. (4) was obtained from the solution of the radiative heat transfer equation system which was numerically solved using the Discrete-Ordinates method (*S*8 approximation) [20]. The radiative heat transfer equation system was closed assuming that, at the IPM surface boundaries, radiative heat exchange occurs with an upstream/downstream blackbody environment at inlet/outlet gas temperature, in agreement with Eqs. (6) and (7).

The combustion chemistry was modeled with a 12-steps C1–C2 reduced reaction mechanism (including 16 species) [21], based on the GRI 2.11 detailed mechanism, see [22].

The thermo-physical properties (ρ_s, C_{ps} and λ_s) of both Al_2O_3 and SiSiC ceramic materials were obtained from [26,27], respectively. The IPM properties of both Al_2O_3 fiber lamellae and SiSiC foam including information for the radiative and convective heat transfer sub-models were obtained from [23–25] and are resumed in Table 2.

An isothermal full 3D simulation, including the porous level structure details, was performed with the Star-CD code [28]. The Al_2O_3 fiber lamellae CAD geometry was overlayed with 2 million nodes. For the SiSiC foam, a MRI sample of 18 cm^3 was obtained (provided by TUBAF [29]) and from that a full 3D mesh of the conical reformer was generated with 5 million cells. Fig. 3a and b depicts the mesh details for the computational models.

For the 3D simulations the flow was also modeled as steady, laminar and incompressible and a second order discretization scheme was employed for the convective term. The relevant boundary conditions corresponds to imposed velocity at the inlet side and pressure at the outlet side, being that the inlet and outlet sections were located far enough from the porous region.

The numerical models were validated against experimental data for the pressure drop. The results for the SiSiC foam also presented a good agreement with the Ergum expression for its equivalent packed bed of spheres.

4. Results

4.1. Al_2O_3 fiber lamellae reformer

After some preliminary simulations of the Al_2O_3 fiber lamellae reformer using the original burner's geometry, it was observed that the *quasi*-1D model predictions for the reaction front location were very much dependent on the power, contrary to the experimental findings [4,18]. The experiments suggested that the reaction front was stabilized in a narrow downstream region of the conical section of the reformer, for a equivalent fuel feed power range from 6 to 30 kW. The one-dimensional assumption is well established for isotropic porous media flows with a dominant fluid flow direction. The Al_2O_3 fiber lamellae presents anisotropic voidage creating fluid flow channeling that counter acts the radial flow spreading due to mass conservation in the diffuser.The *quasi*-1D model obvi-

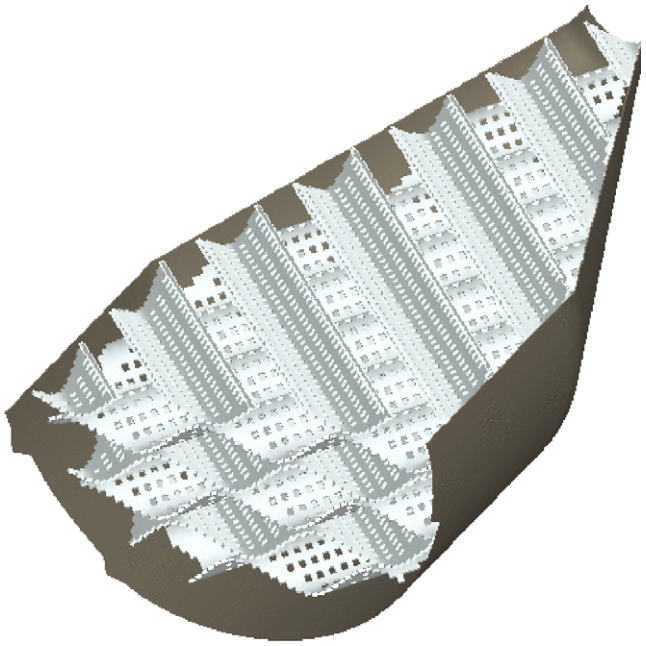

Fig. 4. Al_2O_3 fiber lamellae structure model used in the 3D CFD simulation.

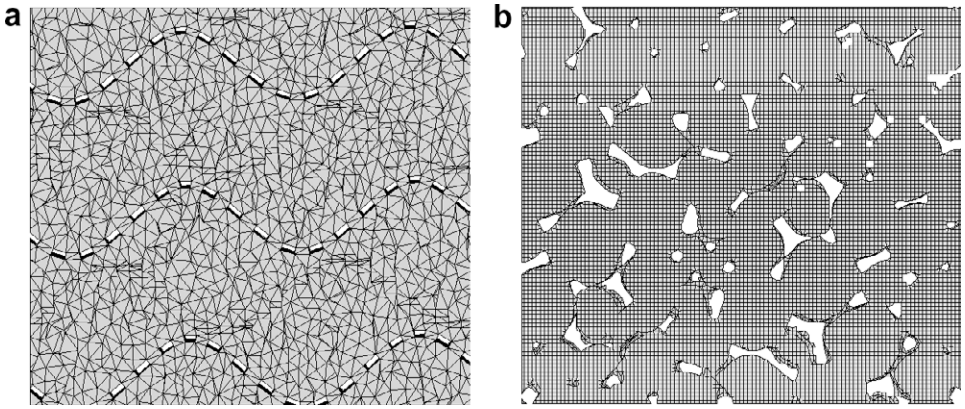

Fig. 3. Numerical 3D meshes of the porous materials: Al_2O_3 fiber lamellae mesh detail (a) and SiSiC porous foam mesh detail (b).

ously can not incorporate the multi-dimensional flow structure in the diffuser region. For the purpose to investigate the flow inside the real lamellae geometry, a full 3D fluid flow analysis was conducted. The full 3D simulation predictions were obtained in order to investigate the validity of using uniform properties in the geometrical cross-sectional area of the diffuser as is inherently assumed in the *quasi*-1D model.

The 3D fluid flow simulation was performed assuming an incompressible flow of air at a fixed inlet temperature of 700 K. The inlet mass flow was chosen to correspond to a typical case of 18 kW, and an inlet averaged Reynolds number of 15,000, based on the characteristic pores size (1.5 cm), was obtained. Fig. 4 shows the fiber lamellae structure used in the simulation.

Fig. 5 shows the velocity magnitude isocontours in the three planes of the diffuser. The 3D flow predictions allows to conclude

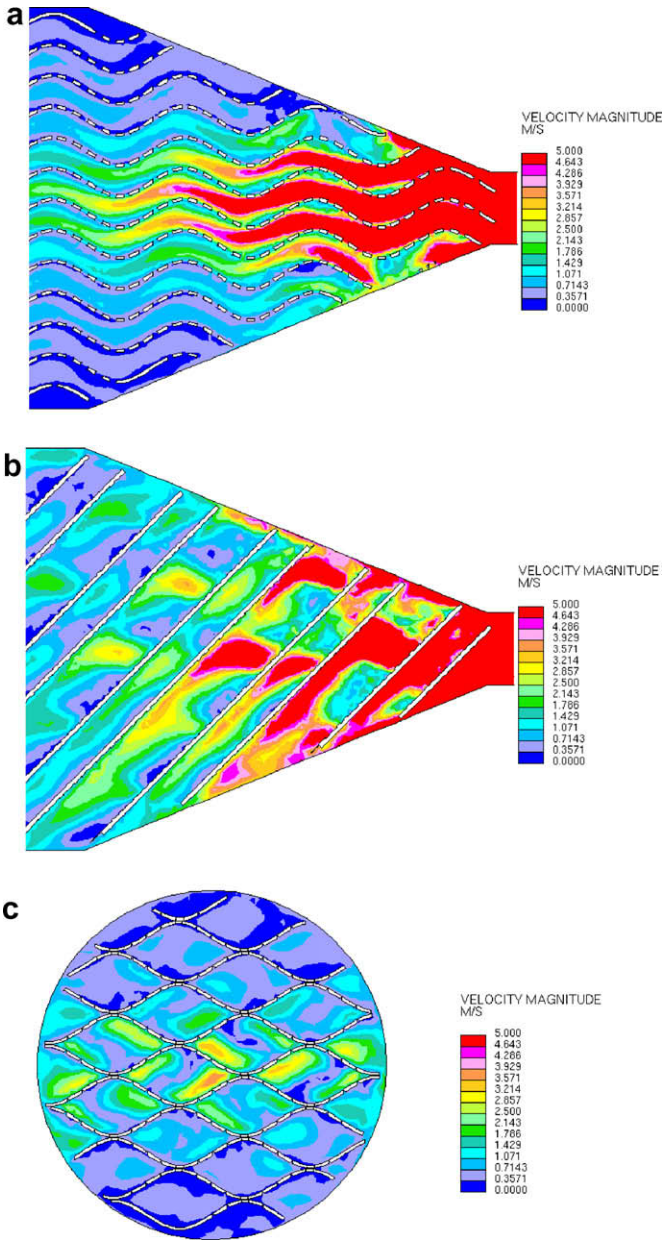

Fig. 5. Fluid flow: on the central section transversal to lamellae structure (a); on the central section parallel to lamellae structure (b); and on a cross-section located at 8.0 cm from the inlet (c).

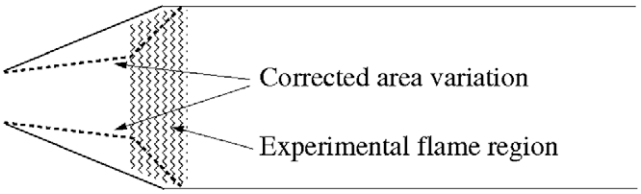

Fig. 6. Diffuser geometries: experimental geometry (original domain) and corrected geometrical domain.

that the fluid flow inside the reformer displays channeling with non uniform velocity in the cross-sectional area variation. The fiber structure induces preferential flow directions, and consequently the fluid flow does not have angular symmetry and is not uniform along the cross-sections of the diffuser. A channeling phenomenon occurs and the tangential average of the multi-dimensional fluid flow behaves like if the area variation was different from a straight wall diffuser.

An inspection of the flow structure in Fig. 5a–c suggests that the flow develops like in a diffuser with two slopes in the wall (see Fig. 6). Inside the first diffuser with a small angle the flow is like a jet while in the second diffuser the flow expands rapidly. If one assumes that the predicted isothermal flow is similar in the combustion case, the cross-sectional area, and volume average variables used in the *quasi*-1D model would reflect the two slope flow expansion.

Based on the above assumption and on the 3D predictions, a geometrical correction was made on the area variation of the *quasi*-1D reformer model, see Fig. 6. The model was assumed to be adiabatic and further simulations, using the corrected geometry, were performed for the Al_2O_3 IPM cases listed in Table 1. Just the higher power cases were considered, for which the adiabatic assumption is better fulfilled in the experiments.

In Figs. 7a and 8a it is presented the comparison between the *quasi*-1D simulation and the experimental centerline temperature and concentration profiles. The originally observed dependence of the reaction front location on the power was strongly eliminated and the steep temperature gradient location is in good agreement with the experiments in an absolute scale of the longitudinal coordinate.

Figs. 7a and 8a show that the predicted temperature profiles are in reasonable agreement with the experimental values. The observed temperature differences can still be caused by uncertainty on the reaction front location, due to the area variation or to the uncertainty on the IPM heat transfer parameters.

The *quasi*-1D model with the chemical kinetics mechanism [21], predicted also very satisfactory the measured species concentrations, see Figs. 7b and 8b, although the CO, H_2 and CO_2 are slightly under predicted and the H_2O is over predicted. The differences observed in the experimental and the simulated main species molar fraction is mainly related with the reaction mechanism used here, which is especially accurate for stoichiometric/lean mixtures, however, it is not optimized for the ultra-rich combustion range [22,30].

Under prediction of CO, H_2 and CO_2, and the over prediction of H_2O are known from previous reforming works where detailed reaction mechanisms (like GRI 2.11; GRI 3.0; NIST) were used, and is justified by the carbon deposition and hydrocarbon synthesis reactions, which are not included, and therefore these reaction models are not able to capture the slow chemistry at lower temperatures existing at ultra-rich conditions [30]. The 12 step reduced mechanism used here is based on GRI 2.11, therefore it suffers from the same problem and a more reliable reaction mechanism for reforming processes may further decrease the

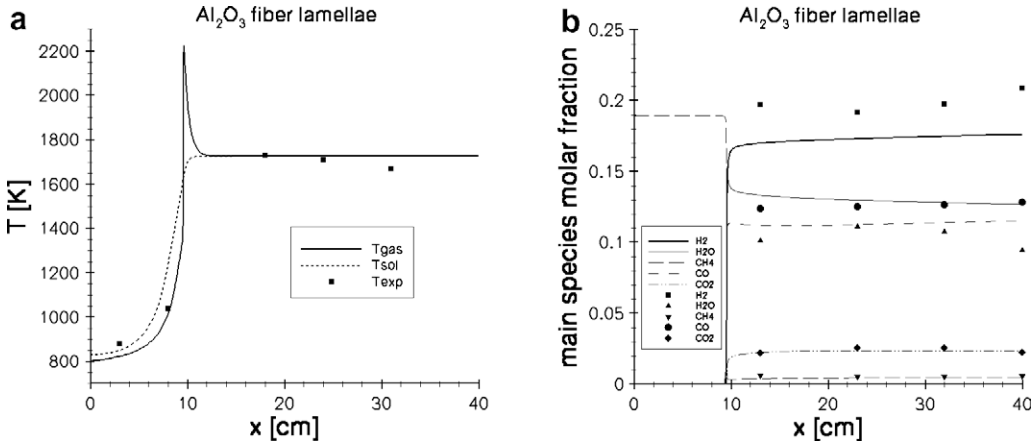

Fig. 7. Temperature and concentration profiles for Case 1: temperature (a); concentration (b).

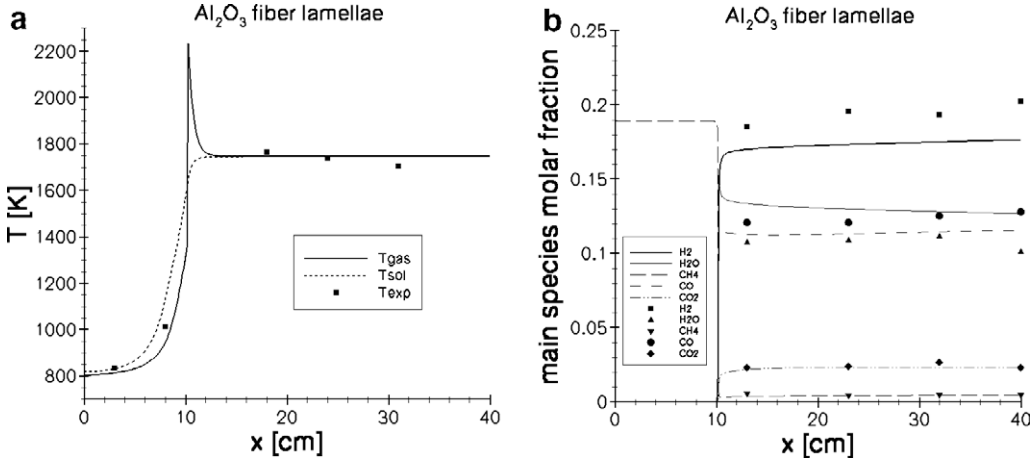

Fig. 8. Temperature and concentration profiles for Case 2: temperature (a); concentration (b).

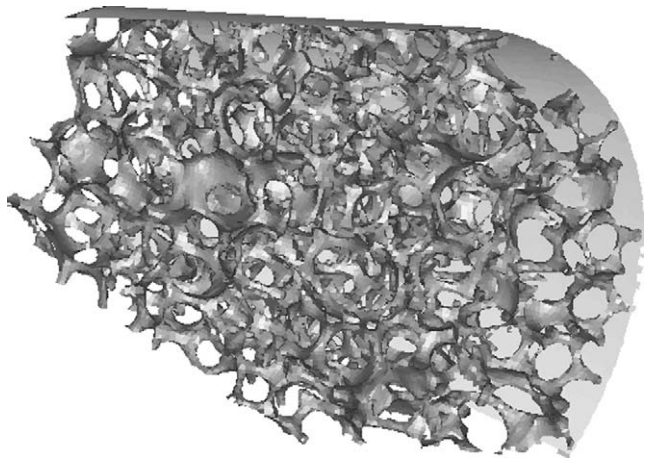

Fig. 9. SiSiC structure model used in the 3D CFD simulation.

small discrepancies found between experiments and numerical predictions.

4.2. SiSiC porous foam reformer

In order to investigate the fluid flow structure inside the SiSiC porous foam a 3D incompressible fluid flow analysis was also performed. Fig. 9 shows a partial section of the porous structure used in the simulation.The detailed porous foam geometry is shown in Fig. 3b, using a computational mesh comprising 5 million unstructured (cartesian) cells.

Fig. 10 show the 3D velocity vector modulus at several diffuser planes. It can be concluded that the fluid flow spreads on the diffuser geometry and does create neither high velocity spot regions nor preferential streams (channeling), contrary to what happened in the Al_2O_3 fiber lamellae case (see Section 4.1). As a consequence, the *quasi*-1D numerical simulation kept the experimental diffuser geometry without any modification or correction.

The comparison between the *quasi*-1D simulation and the experimental centerline temperature and concentration profiles are presented in Figs. 11 and 12, for the SiSiC cases listed in Table 1. Once again, just the higher power cases were considered, for which the adiabatic assumption is better fulfilled in the experiments.

Figs. 11a and 12a show that the experimental temperature profiles are reasonably well predicted by the *quasi*-1D model,

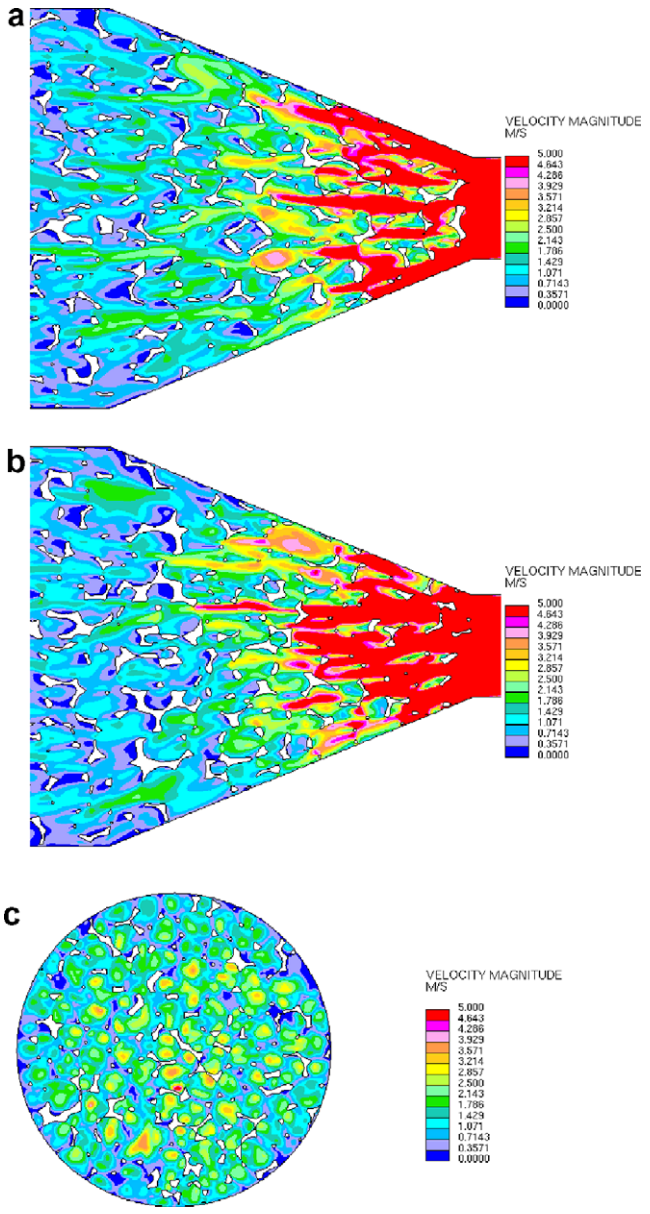

Fig. 10. Fluid flow: on the central section of the SiSiC structure (a); on the central section perpendicular to the previous one (b); and on a cross-section located at 8.0 cm from the inlet (c).

although a small difference in the reaction front location occur, which may be caused by uncertainty on the IPM heat transfer parameters.

It can be observed in Figs. 11b and 12b that the CO, H_2 and CO_2 are under predicted, and the H_2O is over predicted, similar to the Al_2O_3 results. The reason for these discrepancies is related with the range of applicability of the reaction mechanism used here and was already explained above.

5. Conclusions

Quasi-1D numerical simulation of the methane TPOX process within a porous media based reformer, with a geometrical cylindrical diffuser configuration, was validated against concentration and temperature measurements obtained along the centerline of the reactor. Two distinct porous media were considered: the strongly anisotropic Al_2O_3 fiber lamellae structure and the almost isotropic SiSiC foam.

Regarding the Al_2O_3 fiber lamellae structure case, full 3D porous structure isothermal Navier–Stokes simulations were conducted in order to investigate the detailed fluid flow within the reactor. The lamellae structure induced strong flow channeling that can be effectively described for a simplified 1D calculation as being equivalent to the flow inside a double slope diffuser shape. The *quasi*-1D model of the reacting flow with the real diffuser geometry originated a strong dependence of the reaction front on the power and consequently a strong disagreement with the experimental measurements. However, by assuming a double slope diffuser geometry, this simplified model allowed satisfactory agreement for the reaction front and its little influence on the power in the investigated range from 15 to 20 kW (nominal power loads in the cylindrical section in the range of 2 MW/m^2).

For the SiSiC foam case, the *quasi*-1D model predicted very satisfactory the experimental results while keeping the real cross section area variation of the diffuser. Inspection of the isothermal fluid flow Navier–Stokes 3D calculations showed a flow structure without channeling and almost isotropically distributed radially and tangentially in the diffuser. This explains the realistic *quasi*-1D representation of the process in the range from 15 to 22 kW (nominal power loads in the cylindrical section in the range of 2 MW/m^2).

The numerical simulation have reproduced satisfactory the experiments, therefore, it can be concluded that the 3D/1D coupling concept presented here can simplify the modeling of porous media reactive systems, strongly reducing the computation time for the non-feasible 3D full porous structure with detailed chemistry.

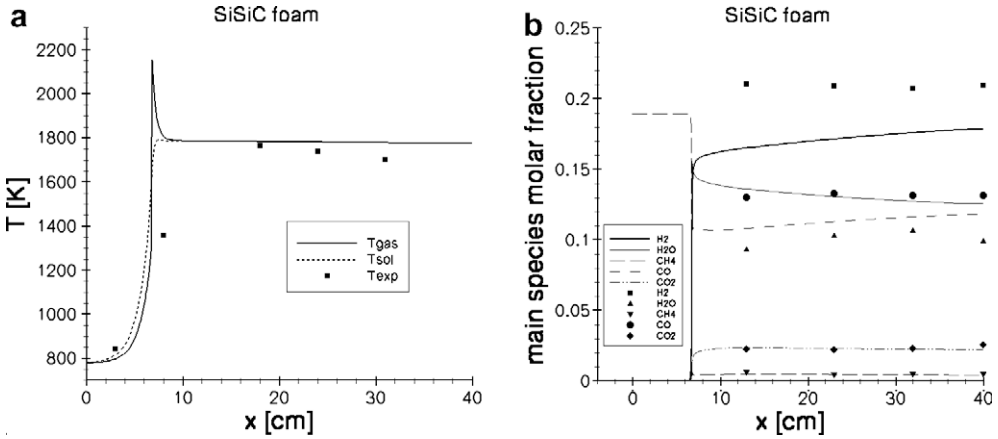

Fig. 11. Temperature and concentration profiles for Case 3: temperature (a); concentration (b).

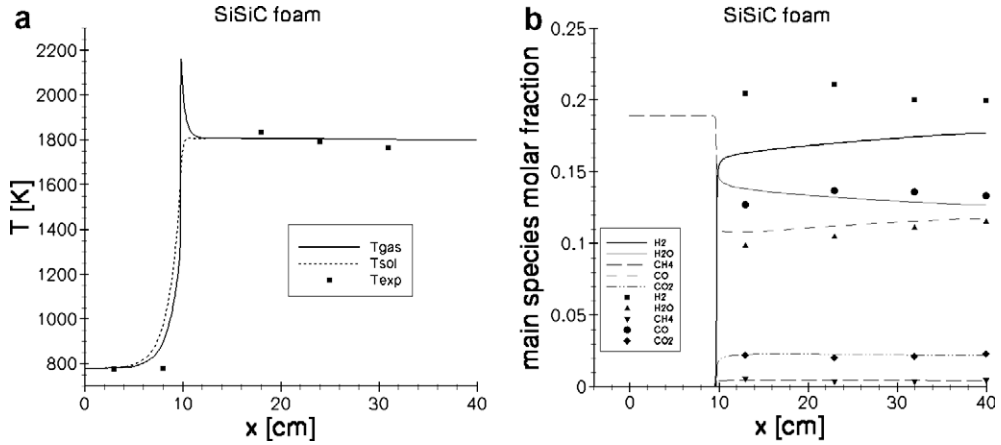

Fig. 12. Temperature and concentration profiles for Case 4: temperature (a); concentration (b).

Acknowledgements

It is gratefully acknowledged the support from EU under the FlameSOFC integrated project (Contract No. FP6-2004-EN3-019875).The first two authors acknowledge the fellowships received from Fundação para a Ciência e a Tecnologia – FCT.

References

[1] Kothari R, Buddhi D, Sawhney RL. Comparison of environmental and economic aspects of various hydrogen production methods. Renew Sustain Energy Revi 2008;12:553–63.
[2] Kumar R, Ahmed S, Krumpelt M. The low-temperature partial-oxidation reforming of fuels for transportation fuel cell systems. In: Fuel cell seminar, Orlando, 1996.
[3] Tindall B, Crews M. Alternative technologies to steam-methane reforming. Hydrocarbon Process 1995:74.
[4] Al-Hamamre Z, Voss S, Trimis D. Hydrogen production by thermal partial oxidation of hydrocarbon fuels in porous media based reformer. Int J Hydrogen Energy 2009;34:827–32.
[5] Pedersen-Mjaanes H, Mastorakos E. Hydrogen production from rich combustion in porous media. Int J Hydrogen Energy 2005;30:579–92.
[6] Barra AJ, Ellzey JL. Heat recirculation and heat transfer in porous burners. Combust Flame 2004;137:230–41.
[7] Trimis D, Wawrzinek K. Flame stabilization of highly diffusive gas mixtures in porous inert media. J Comput Appl Mech 2004;5:367–81.
[8] Trimis D, Durst F. Combustion in a porous medium-advances and applications. Combust Sci Technol 1996;121:153–68.
[9] Hackert CL, Ellzey JL, Ezekoye OA. Combustion and heat transfer in model two-dimensional porous burners. Combust Flame 1999;116:177–91.
[10] Farzaneh M, Ebrahimi R, Shams M, Shafiey M. Numerical simulation of thermal performance of a porous burner. Chem Eng Process 2009;48:623–32.
[11] Hayashi TC, Malico I, Pereira JCF. Three-dimensional modelling of a two-layer porous burner for household applications. Comput Struct 2004;82:1543–50.
[12] Al-Hamamre Z, Voss S, Al-Zoubi A, Trimis D. Experimental and numerical investigation of the partial oxidation of methane in a porous reactor. In: 9th Conference on energy for a clean environment, Lisbon, Portugal, July, 2007.
[13] Malico I, Zhou XY, Pereira JCF. Two-dimensional numerical study of combustion and pollutants formation in porous burners. Combust Sci Technol 2000;152:57–79.
[14] Brenner G, Pickenäcker K, Pickenäcker O, Trimis D, Wawrzinek K, Weber T. Numerical and experimental investigation of matrix-stabilized methane/air combustion in porous inert media. Combust Flame 2000;123:201–13.
[15] Zhou XY, Pereira JCF. Numerical study of combustion and pollutants formation in inert nonhomogeneous porous media. Combust Sci Technol 1997;130:335–64.
[16] Dhamrat RS, Ellzey JL. Numerical and experimental study of the conversion of methane to hydrogen in a porous media reactor. Combust Flame 2006;144:698–709.
[17] Kaviany M. Principles of heat transfer in porous media. 2nd ed. New York: Springer-Verlag; 1995.
[18] Al-Hamamre Zayed. Development of a small-scale multi-fuel processor for synthesis gas production by thermal partial oxidation. PhD Dissertation, Technische Universitaät Bergakademie Freiberg, Germany, 2008.
[19] Kee RJ, Grcar JF, Smooke MD, Miller JA. A fortran program for modelling steady laminar one-dimensional premixed flames. Report SAND85-8240, Sandia National Laboratories, 1996.
[20] Modest MF. Radiative heat transfer. New York: McGraw-Hill; 1993.
[21] Barlow RS, Karpetis AN, Frank JH, Chen JY. Scalar profiles and NO formation in laminar opposed-flow partially premixed methane/air flames. Combust Flame 2001;127:2102–18.
[22] GRI mech. web site: <http://www.me.berkeley.edu/gri mech>.
[23] Scheffler M, Colombo P. Cellular ceramics: structure, manufacturing, properties and applications. Wiley-VCH, Weinheim; 2005.
[24] Ellzey JL, Howell JR, Hall MJ. Combustion of hydrocarbon fuels with porous inert media. Progress Energy Combust Sci 1996;22:121–45.
[25] Pickenäcker K. Emissionsarme kompakte gasheizsysteme auf der basis stabilisierter verbrennung in porösen medien. PhD thesis, University of Erlangen – Nuremberg, Fortshr.-Ber. VDI Reihe 6 Nr. 445, Germany, 2001. ISBN: 3-18-344506-9.
[26] Munro RG. Evaluated material properties for a sintered alpha-Al_2O_3. J Am Ceramic Soc 1997;80:1919–28.
[27] Munro RG. Material properties of a sintered alpha-SiC. J Phys Chem Ref Data 1997;26:1195–203.
[28] Star-CD software web site: <http://www.cd-adapco.com/products/STAR CD/index.html>.
[29] Trimis D. MRI data of a SiC sample. Personal communication, 2007.
[30] Konnov AA, Zhu J, Bromly JH, Zhang DK. Non-catalytic partial oxidation of methane over a wide temperature range. In: Proceedings of the European combustion meeting, 2003.